ACS OMEGA

http://pubs.acs.org/journal/acsodf

Article

Characterization and Quantitation of Carbon Black Nanomaterials in Polymeric and Biological Aqueous Dispersants by Asymmetrical Flow Field Flow Fractionation

Lorenzo Sanjuan-Navarro, Yolanda Moliner-Martínez, and Pilar Campíns-Falcó*

Cite This: *ACS Omega* 2021, 6, 31822−31830

Read Online

ACCESS | Metrics & More | Article Recommendations | Supporting Information

ABSTRACT: Characterization of carbon black (CB) nanomaterials is required in industrial and research areas. Hence, in this study, asymmetrical flow field flow fractionation coupled to UV−vis and DLS detectors in series (AF4-UV−vis-DLS) was studied to evaluate the CB dispersion behavior in polymeric and biological dispersants, given the relevance of these media in practical applications. Under the experimental conditions, the results indicated that polymeric and biological dispersions showed size distributions with hydrodynamic diameters of 404 and 175 nm, respectively, for a particle core diameter of 40 nm. The polymeric dispersant provided lower stability as a function of time than that achieved by the biological dispersant. AF4 allowed separation of different core-sized CB (40, 69, and 72 nm) according to their hydrodynamic size using cross-flow rates of 0.5 mL·min^{-1} and 1 mL·min^{-1} for polymeric and biological dispersants, respectively. The dilution of the polymeric dispersion with different real water matrices produced a dramatic loss of dispersion stability, this effect being negligible in the case of biological dispersions.

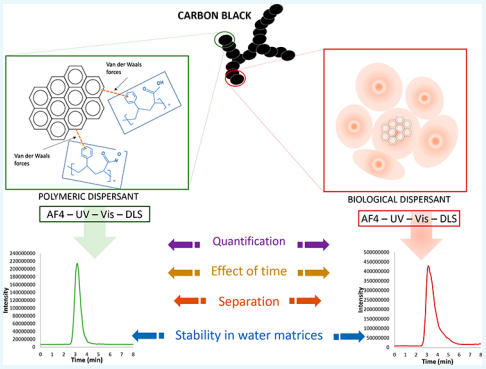

INTRODUCTION

Carbon black (CB) is a quasi-graphitic form of almost pure elemental carbon, which is produced commercially under controlled conditions from incomplete combustion of aromatic hydrocarbons at a high temperature. The synthetic process generates a wide variety of particles with different characteristics of particle size, surface area, structure, and surface chemistry, which are important with regard to the current CB applications.[1−3]

CB as pigments[4] or nanofillers[5] has given rise to interesting areas of research. Moreover, its versatility, electrical conductivity, and easy functionalization make it one of the most common materials used for improving different industrial products and compounds in several areas. CB is used in a variety of essential items[6] such as tires, plastics, food contact specific grades, batteries, high-performance coatings, rubber goods, pipes, agricultural irrigation, mulch films and greenhouse covering, automobile skin contact, wires and cables, and toner and printing inks. Among these, specific mention can be made of incorporation into rubbery polymers to increase mechanical properties.[7] CB is also of use in electrochemical (bio)sensors for environmental contaminants and enzymes.[8,9] The improvement of nanofibers and nanocellulose composites containing nanofibrils and nanocrystals has also been carried out by using CB.[10,11] In addition, CB is an important material as a support in electrochemical catalytic systems.[12,13]

On the other hand, toxicological studies using CB as a model particle have been reported to simulate environmental carbonaceous particles in medical and health science.[14,15] These studies lead to establish its possible toxicological effect in cells or organisms.

The development of methodologies to characterize and quantify CB for obtaining reliable information is a challenge in analytical chemistry. From an analytical point of view, interest lies in matrices such as industrial, environmental, and biological samples, taking into account applications indicated in the previous paragraphs.

Taking into account the different scenarios where CB is of interest, polymeric and biological dispersants have been widely used. In aqueous media, polymeric dispersants interact with the CB surface via different electrostatic forces to build voluminous shells or intensify charges around the surface, preventing nanoparticle flocculation, coagulation, and aggregation, thereby allowing their dispersion.[16] Thus, ink industry,[17−21] fiber research studies,[22] and electrochemical studies[23] use these dispersants in their procedures. On the

Received: August 19, 2021
Accepted: November 2, 2021
Published: November 18, 2021

other hand, CB dispersions in cell cultures have also been proposed for biological analysis and toxicology studies.[24−27] However, CB aqueous dispersions are limited due to their low stability and homogeneity. Therefore, a deeper knowledge about CB dispersions is demanded in research and industrial applications to achieve reliable information.

Imaging techniques such as transmission electron microscopy (TEM) and scanning electron microscopy (SEM)[28,29] and optical techniques, mainly dynamic light scattering (DLS),[30,31] have been proposed to determine the physical and morphological properties such as particle size, hydrodynamic diameter, or surface structure. On the other hand, Raman spectroscopy, UV−vis spectroscopy, and electrochemical impedance spectroscopy have been used to evaluate chemical structures[32] for characterization of surface modification[30] and nonaqueous dispersions,[33] respectively. These techniques have proven to provide relevant information about important properties of CB. However, CB analysis using the abovementioned techniques is limited since size distribution and composition information are not obtained simultaneously. For this aim, a separation technique is needed in order to achieve an accurate particle size distribution. Indeed, separation techniques based on different principles are getting more relevance in nanomaterial field in general and in particular for CB characterization and determination.

In this context, electrophoresis has been proposed for quantification studies on biological samples;[24] however, size distribution is not defined. For this aim, asymmetrical flow field flow fractionation (AF4) has been demonstrated to be a powerful separation strategy in the characterization and/or determination of several (nano)materials.[34,35] AF4 coupled to UV−vis and DLS detectors in series is a very useful technique for characterization of a wide range of particle dispersions allowing their separation and establishing their distribution and stability.[36,37] The AF4-UV−vis system was employed to analyze only the size of CB particles used in ink by dispersing CB powder in aqueous media containing polymeric dispersants.[38] However, stability studies on different dispersant matrices have not been yet performed for CB. AF4 can determine the suspension behavior through the separation of different size distributions present in the bulk dispersion and allows quantification studies.

Thus, the objective of this study is to evaluate stability and fully characterize polymeric and biological CB dispersions by using the AF4-UV−vis-DLS. Size and composition distributions have been studied under different experimental conditions as a function of peak symmetry, sensitivity, precision, and resolution. The fractogram profiles have been studied in different real water samples as an stability application example to study the influence of dispersive media in environmental analysis due to the growing concern about this nanoscale material in the environment.

RESULTS AND DISCUSSION

Characterization of Several Solid CB Samples. Characterization of solid nanoCB bulk samples (N326, N550, and N722) was performed by SEM, TEM, and Raman spectroscopy. TEM microscopy was used to estimate the average core size of these nanoparticles. The measurements revealed particles sizes of 40, 69, and 72 nm for N326, N550, and N722, respectively. These results were in concordance with the specific surface area values given by the manufacturer. As it was expected, N550 and N722 showed a similar specific surface area (SSA) and SSA for N326 was higher, which was correlated with a smaller particle size.

The particle size obtained by TEM measurements also correlated with the size obtained by SEM analysis. Figure 1a.1−a.3 shows the micrographs obtained with SEM for N326, N550, and N722, respectively. The morphology of particles was similar and aggregates of spheroidal and ellipsoidal primary particles were present in all cases.

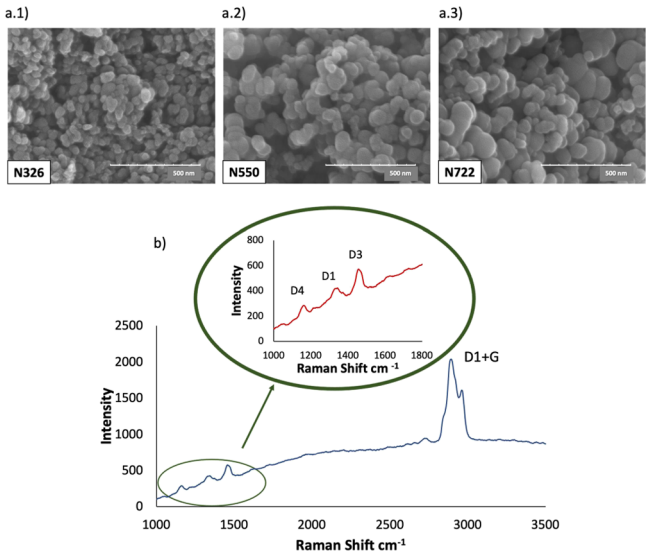

Figure 1. SEM micrographs of (a.1) N326, (a.2) N550, and (a.3) N722. (b) Raman spectra of CB N326. The inset shows the characteristic Raman bands between 1000 and 1500 cm^{-1}.

Different Raman bands were observed in the analysis of the N326 sample. The presence of bands at 1300 cm^{-1} (D1) and 2950 cm^{-1} (D1 + G) was in agreement with the CB structure. Moreover, the band D3 at 1500 cm^{-1} corresponded to amorphous carbon. In particular, band D3 can be related to the amount of sp3 carbon between sp2 carbon rings, and the D4 band was attributed to hydrocarbon components or aliphatic moieties grafted. Similar bands were observed for samples N550 and N722, which corroborates possible CB structures.[39]

Characterization of nanoCB Dispersions. Taking into account some scenarios where CB can be an analyte of interest[17,22,23,27] as mentioned in the Introduction section, both polymeric and biological dispersants were studied (see Materials and Methods Section for preparation). Figure 2a,b shows the optical microscopy images of CB dispersions in each dispersant, respectively. This technique was used for characterizing the bulk dispersion; particularly, self-assembly droplets within the μm interval constitute its external structure in the case of a biological dispersant, which contained a surfactant in its composition, Tween 80, too.

In this study, a mixture of acrylic acid and styrene was used as a polymeric dispersant since it has been demonstrated to be used as a dispersant that can confer stability and low viscosity to the dispersion. The mechanism involved is schematized in Figure 2c. The structure was a random copolymer containing polar and nonpolar moieties. As the polar part, acrylic acid provided solubility in water. Other monomers acting as nonpolar parts, such as styrene, bind with nanomaterials mainly through van der Waals forces. Hydrogen bonds between carboxyl groups present in the material surface and polymer were also done.[40] When a dispersant contains both

https://doi.org/10.1021/acsomega.1c04527
ACS Omega 2021, 6, 31822−31830

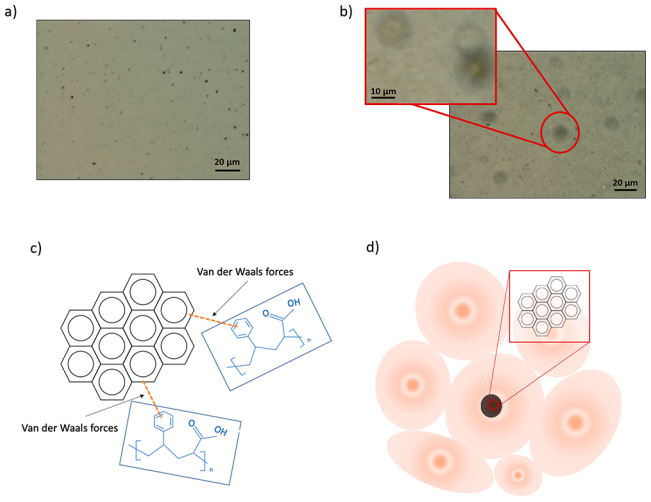

Figure 2. Optical microscopy images of CB dispersions in (a) polymeric and (b) biological dispersants. Mechanism involved in the dispersion of CB using (c) polymeric dispersant and (d) biological dispersant.

polar and nonpolar components such as these considered, it can stabilize CB particles in water, working as a type of surfactant.[17,20] Pigment dispersion was usually stabilized in water via the electrostatic repulsion of charges.[17,20,23,41]

On the other hand, the biological dispersant studied in this study is based on a cell culture media. This dispersant was a high ionic strength solution, buffered at physiological pH and containing different proteins or nutrients, Tween 80 and supplemented with L-alanyl-L-glutamine dipeptide in one of the two studied media. These compounds contribute to the CB capping, mainly proteins.[42,43] The self-assembly droplets provided an external environment for CB capping, and the schematic diagram is shown in Figure 2d. It should be noted that these structures were not observed in the case of polymeric dispersant.

A TEM analysis was carried out to establish the different CB structures present in both dispersions. Moreover, AF4-DLS measurements were performed at different concentration levels in order to test linearity for quantitation purposes and study the main size populations. Sample N326 was selected as the target analyte.

The structure size of CB dispersions has a significant impact on the nanomaterial properties. Typically, primary particles combine to form aggregates of different sizes and agglomerates.[44] As can be seen in Figure 3, TEM images allowed the observation of different forms of aggregates and agglomerates in the bulk dispersions. For the polymeric dispersant, Figure 3a,b shows primary particles dispersed individually. Meanwhile, Figure 3c,d shows several aggregates with linear, spherical, and ramified forms present in the polymeric dispersion.

Similarly, the biological dispersion showed a variety of structures. In Figure 3e, the dispersion of different individual particles can be observed. Figure 3f,g shows some linear, spherical, and elliptic structure forms. Meanwhile, in Figure 3h, a spherical agglomerate with a size larger than 200 nm composed of different individual particles is observed.

Using the polymeric dispersant, different CB dispersions from sample N326 were prepared and analyzed using the AF4-DLS system using a cross-flow of 0.5 mL·min^{-1} and in batch DLS. Figure 4a,b shows the obtained fractograms, which

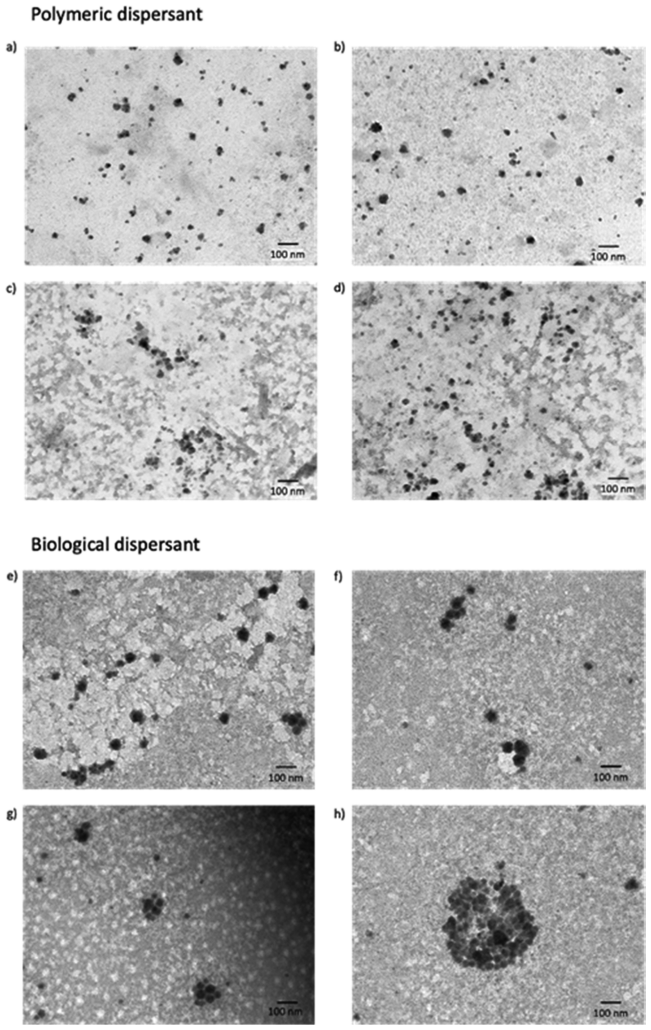

Figure 3. TEM images of CB structures in (a–d) polymeric dispersion and (e–h) biological dispersion.

provided a linear relationship between peak area versus concentration with a satisfactory regression coefficient (R^2 = 0.99). In terms of peak characteristics, a symmetric well-defined profile was obtained. Table 1 shows the width at half-height and the tailing factor for each dispersant. The calculated tailing factor for the polymeric dispersant was 1.64 and it can be correlated with the level of monodispersity provided. TEM micrographs were in agreement with the results since mainly homogeneous particles can be observed (core size of 40 nm) (Figure 4b).

The same study was carried out using a biological dispersant and sample N326 as the target CB too. Two biological media were studied, Tween 80 + DMEM/F-12 and Tween 80 + DMEM/F-12 supplemented with L-alanyl-L-glutamine (see Materials and Methods Section). The resulting dispersions and their dilutions were injected in the AF4-UV–vis-DLS system using a cross-flow of 0.5 mL·min^{-1} (Figure 4c,d). As can be seen, the use of this dispersant also resulted in a single peak but with a higher width than that obtained with the polymeric dispersant. The tailing factor in this case was 4.9, which was attributed to a wide size distribution in the biological medium. Indeed at 36.2 mg·L^{-1}, a peak shoulder was observed in the AF4-DLS peak.

https://doi.org/10.1021/acsomega.1c04527
ACS Omega 2021, 6, 31822–31830

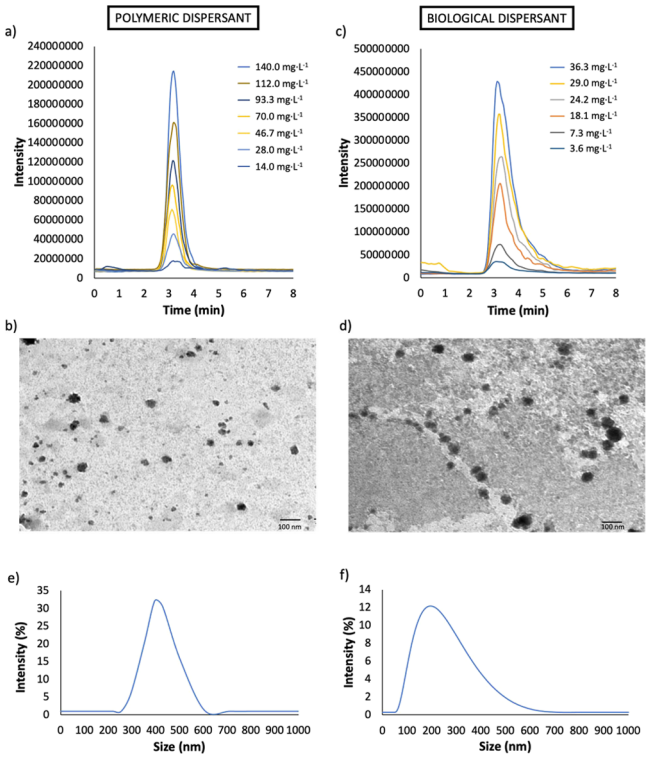

Figure 4. Results obtained for CB dispersion from sample N326 prepared in both studied dispersants. (a) DLS fractograms at different concentration levels using the biological supplemented dispersant with the L-alanyl-L-glutamine dipeptide. (b) TEM image of CB dispersion in the biological dispersant. (c) Zeta potential and hydrodynamic diameter results obtained by DLS analysis in batch and AF4-DLS using polymeric and biological dispersants. (d) DLS fractograms at different concentration levels using the polymeric dispersant. (e) Histogram−DLS measurement in batch of polymeric dispersion. (f) Histogram−DLS measurement in batch of biological dispersion.

Table 1. Peak, Physical, and Analytical Parameters for Sample N326 in Polymeric Dispersant and Biological Supplemented Dispersant

	dispersants	
parameters	polymeric	biological
peak		
width half-height, $W_{1/2}$ (min)	0.63	0.82
tailoring factor	1.64	4.9
physical		
d_{hydro} (nm) (DLS)	404 ± 4	175 ± 4
d_{hydro} (nm) (AF4-DLS)	387 ± 6	175 ± 3
$Z_{potential}$ (mV)	23 ± 2	−19 ± 1
analytical		
sensitivity ($mg^{-1}·L$)	$(1.5 \pm 0.8) \times 10^6$	$(1.22 \pm 0.07) \times 10^7$
LOD ($mg·L^{-1}$)	1.38	0.16
precision, RSD (%)	5.0	1.7

Precision studies were also carried out for this purpose, and the relative standard deviation (% RSD) was calculated. The results obtained for three replicates showed that RSD values were lower than 5% for the CB polymeric dispersion and 1.74% for the CB biological dispersion (see Figure S1 in the Supporting Information, SI). The precision achieved by the biological dispersant was better than that obtained by the polymeric dispersant.

Batch DLS measurements (% intensity vs particle size) are shown in Figure 4e,f for both dispersions. A wider size distribution was obtained for CB in the biological medium compared with the polymeric one. Table 1 shows the hydrodynamic diameters, both from AF4-DLS and in batch DLS mode providing similar values. A single population with the calculated size is the predominant one in dispersions. The hydrodynamic diameter (d_{hydro}) for CB dispersed in the biological dispersant has a value of 175 nm. Similar sizes were obtained for the cellular dispersant without the supplement (see Figure S2 in the SI) although the signals of the fractograms were smaller than that obtained with the more complex cellular dispersant. For the polymeric agent, d_{hydro} was 404 and 387 nm in batch and AF4-DLS, respectively, indicating a smaller dispersion capacity that that achieved by the biological dispersant.

Zeta potential was also measured (see Table 1), providing positive values for the polymeric dispersant, which were in agreement with the polymer charge, and negative values for the biological dispersant related to the chemical structure of the biological medium. The cellular dispersant without a supplement provided values of zeta potential around −12 mV (see Figure S2 in the SI) instead of −19 mV provided by the cellular dispersant with the L-alanyl-L-glutamine dipeptide.

Furthermore, linear calibration graphs were obtained with a satisfactory regression coefficient ($R^2 > 0.995$). The slope obtained for the CB biological dispersant was $(1.22 \pm 0.07)\cdot\times 10^7$ $mg^{-1}·L$ in a working concentration range of 3.6 to 36.3 $mg·L^{-1}$. Meanwhile, the value for the CB polymeric dispersion was $(1.5 \pm 0.8) \times 10^6$ $mg^{-1}·L$, in a concentration range of 14.0 to 140.0 $mg·L^{-1}$. Thus, the use of the biological dispersant gave rise to higher sensitivity. This means that detection limits for CB were lower by employing the biological dispersant. As can be seen in Table 1, LOD for the CB biological dispersion was 0.16 $mg·L^{-1}$ and for CB polymeric dispersion, it was 1.38 $mg·L^{-1}$.

The presence of the L-alanyl-L-glutamine dipeptide in the biological medium gave rise to an increase in CB dispersion. In order to prove this, a biological medium without this additive was studied in the same working concentration range. DLS fractograms provided satisfactory regression with a slope of $(9.9 \pm 0.3) \times 10^6$ $mg^{-1}·L$. The results indicated that the slope was higher in the presence of L-alanyl-L-glutamine (see Table 1), which meant an increase in dispersed CB. In addition, the peak width and tailoring factor were similar in both cellular media (see Figure S2 in the SI).

The stability of CB dispersion was studied for N326 CB using the biological supplemented dispersant. The slopes of the linear equation within the intervals 1.9−9.6 and 0.60−2.75 $mg·L^{-1}$ were $(1.13 \pm 0.04) \times 10^7$ and $(1.15 \pm 0.08) \times 10^7$ $mg^{-1}·L$, respectively. These results indicated that biological CB dispersion showed suitable dispersion stability in a wide concentration range since no significant differences were found. For N550 and N722, similar results were obtained.

Effect of Time on the Analytical Response of NanoCB Dispersions. Figure 5a shows the % DLS fractogram signal for CB (N326) dispersion with polymeric and biological dispersants using as a reference the intensity obtained for CB dispersion at day 0 considered as a fresh dispersion.

As it can be seen, for the polymeric dispersant, the results indicated that the DLS fractogram decreased as a function of

https://doi.org/10.1021/acsomega.1c04527
ACS Omega 2021, 6, 31822−31830

a)

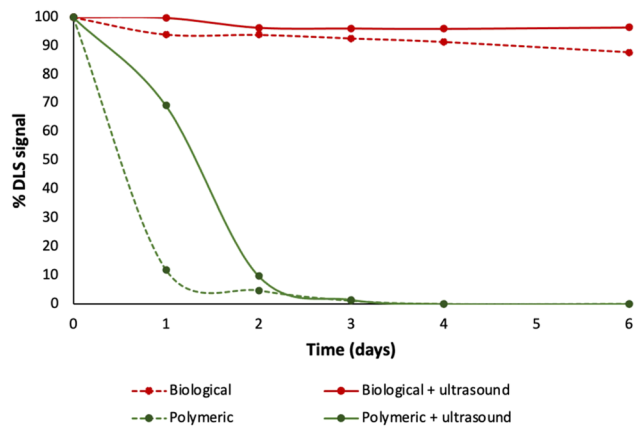

b)

Size (nm)	N326			
	Day 0	Day 1	Day 2	Day 6
Polymeric	386.6	432.3	2360	---
Biological	175.4	179.4	177.3	183.2

Figure 5. (a) % DLS fractogram signal (using as a reference the dispersion of day 0) obtained as a function of dispersion preparation time for CB N326 with two studied dispersants: polymeric (green) and biological (red), using ultrasound (continuous line) and without ultrasound (dashed line) before injection. (b) Particles sizes obtained with the AF4-DLS for each dispersant as a function of dispersion time after the ultrasound step.

time. 90% of the signal was lost in 1 day, showing low stability in this dispersion medium. An ultrasound treatment of these dispersions before the injection only improved the signal reduction by 70%. Particle sizes for different CB dispersions on different days were analyzed (after the ultrasound treatment), see Figure 5b. For the CB polymeric dispersion, the particle size increased as the stability decreased, which corroborated the aggregation of CB.

On the other hand, a stable dispersion was obtained for the CB biological dispersant since the signal was constant over time. In this case, the CB size was between 175 and 180 nm as a function of time, demonstrating the stability of CB in this dispersant.

CB Separation. In order to evaluate CB separation with the AF4-UV−vis-DLS, three different CB samples (N326, N550, and N722) were dispersed using both dispersants, biological and polymeric, following the procedure described in the Materials and Methods Section. First, CB dispersions of the three samples were analyzed by DLS in batch mode (see Table 2). As can be seen, d_{hydro} for N326 was the lowest in both dispersants, which was related to the minor core size. On the other hand, N550 exhibited the highest d_{hydro} with a significant difference with respect to N722 although both of them showed a similar core size. This fact was attributed to the high oil absorption number (OAN) of sample N550, resulting in a greater capping layer of both dispersants, and thus a higher hydrodynamic diameter compared with N326 and N772.[45]

The zeta potential was also measured for CB samples, showing similar results for the different CBs. In AF4, one of the most important parameters is the cross-flow rate, which determined the resolution. In this study, two different cross-flow rates were applied to study the CB separation depending

Table 2. Particle Size (d_{hydro}) and Zeta Potential of Different CB Nanoparticle Dispersions (N326, N550, and N722) Using Polymeric and Biological Dispersants[a]

		N326	N550	N722
polymeric dispersant	size batch DLS (nm)	404.0	731.5	662.4
	size AF4-DLS (nm)	386.6	720.2	667.5
	zeta potential (mv)	22.6	20.4	22.9
biological dispersant	size batch DLS (nm)	175.5	540.6	351.8
	size AF4-DLS (nm)	175.4	544.1	357.2
		178.4*	538.2*	344.5*
	zeta potential (mv)	−18.8	−16.9	−17.0

[a]Fractograms were obtained at 0.5 mL min^{-1} except for * at 1.0 mL min^{-1}.

on the dispersant used. Figure 6 shows the UV−vis fractograms of different CB dispersions for polymeric and biological dispersants with cross-flow rates of 0.5 and 1.0 mL·min^{-1}.

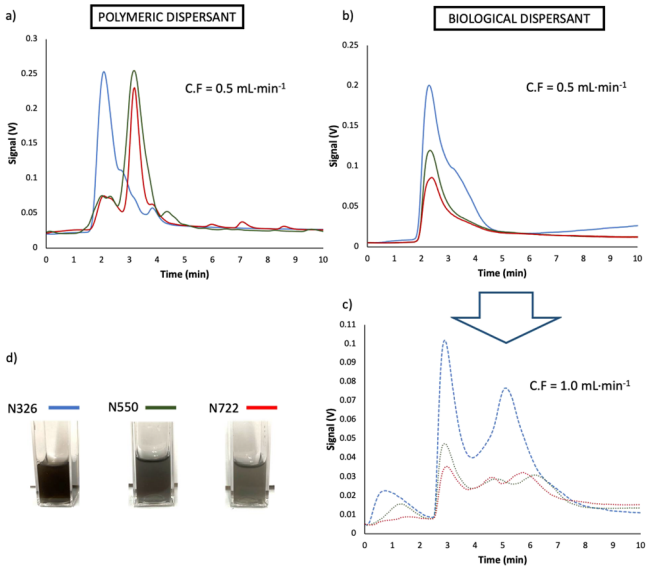

Figure 6. UV−vis fractograms obtained for CB dispersion (N326 in blue, N550 in green, and N722 in red) at different cross-flow rates: (a) polymeric dispersion CB analysis using a cross-flow rate of 0.5 mL·min^{-1} and biological dispersion CB analysis using cross-flow rates of (b) 0.5 mL·min^{-1} and (c) 1.0 mL·min^{-1}. (d) Visual color representation of each CB biological dispersion.

Figure 6a shows the fractogram for several CB samples at 140 mg·L^{-1} in the polymeric dispersant at a cross-flow rate of 0.5 mL·min^{-1}. N326 was identified at time 1.9 min corresponding to the void peak. Meanwhile, N550 and N722 were separated at a higher time (2.9 min). As it was expected, N550 and N722 were not resolved due to their similar particle size. For all of them, small peaks appeared in the fractograms that were compatible with aggregates or agglomerates of CB. The use of a higher cross-flow rate with the polymeric dispersant did not provide satisfactory results due to the lack of stability.

Figure 6b,c shows the fractograms for CB biological dispersion (36 mg·L^{-1}) for the three CB samples assayed at two cross-flow rates of 0.5 and 1 mL·min^{-1}. N326 provided a peak and a shoulder at 0.5 mL·min^{-1}. By using a cross-flow rate of 1.0 mL·min^{-1}, suitable separation from the void peak was

https://doi.org/10.1021/acsomega.1c04527
ACS Omega 2021, 6, 31822−31830

achieved: peaks at 5.1, 5.7, and 6.2 min correspond to N326, N772, and N550, respectively. Furthermore, d_{hydro} values of the three CB samples using the AF4 system for both cross-flow rates assayed were in agreement with the results provided by batch DLS measurements (see Table 2). Figure 6d shows an image of each CB dispersion at the same concentration level, with their colors being directly related with the intensities obtained from AF4-DLS fractograms.

Stability of Dispersions by Dilution in Real Waters. As a practical case of study, CB dispersion by dilution in several water matrices was performed taking into account the potential occurrence of these nanomaterials in the environment. For this aim, diluted dispersions were prepared with real water matrices (dilution factors of 1/2 and 1/8 for CB (N326) polymeric and biological dispersants, respectively). Figure 7a shows characterization parameters for each water matrices used: conductivity, sulfate, and nitrate. As it was expected, the highest values were obtained for the wastewater sample.

a)

	pH	Conductivity (μs/cm)	Turbidity (NTU)	NO_3^- (mg/L)	SO_4^{2-} (mg/L)
Tap Water	8.08	943	0.1526	7.32	266.25
Well Water	7.64	1091	0.2201	55.54	307.26
Waste Water	7.98	2600	0.5300	192.52	873.18

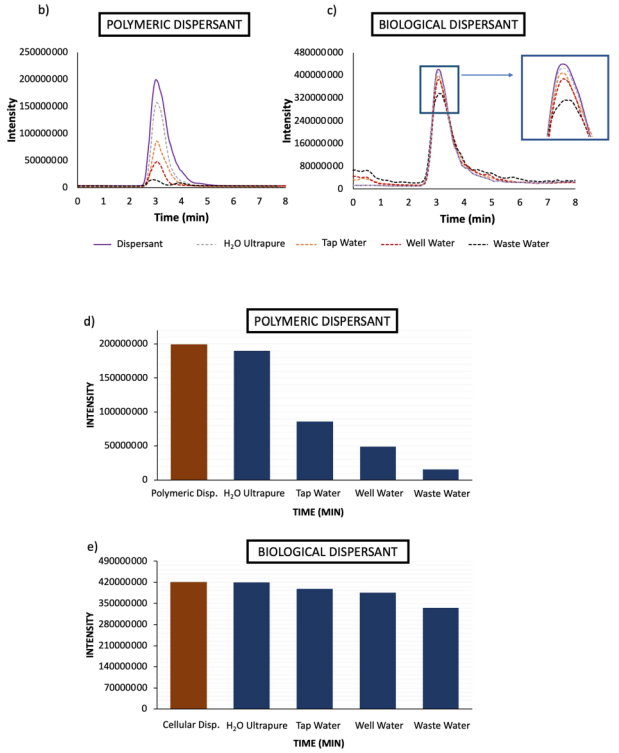

Figure 7. (a) pH, conductivity, turbidity, nitrate, and sulfate values for each aqueous matrices. (b) DLS fractograms at 0.5 mL min^{-1} with different water matrices as final dilution media for polymeric dispersions. (c) DLS fractograms at 0.5 mL min^{-1} with different water matrices as final dilution media for biological dispersions. (d) Maximum intensity obtained in DLS fractograms analysis for each CB dispersion diluted with different water matrices using the polymeric dispersant. (e) Maximum intensity obtained in DLS fractograms analysis for each CB dispersion diluted with different water matrices using the biological dispersant.

In polymeric CB dispersions (Figure 7b), an increase in turbidity and conductivity occurred due to the presence of high amount of anions, producing a dramatic loss of dispersion stability. This effect was more remarkable for CB-diluted dispersion in wastewater than that produced in the other water matrices, its signal being reduced up to 90% as Figure 7d shows. When ultrapure water was used to prepare diluted dispersions, the stability of CB dispersion was not altered. In the case of CB biological dispersions, dilution with different waters did not induce a significant signal decrease (see Figure 7c,e).

This study demonstrates the influence of the sample matrix on the stability of dispersion as a function of the CB dispersive agents. Therefore, the success in the determination of the CB size and composition distribution will depend on the analytical strategy that takes into account the dispersion performance of these compounds.

CONCLUSIONS

In this study, polymeric and biological dispersants were studied in order to evaluate their capability to disperse CB nanomaterials. The dispersion mechanism proposed showed that polymeric dispersion was achieved through van der Waals forces between nanomaterials and copolymers used, while the biological dispersant formed capping with biomolecules, mainly amino acids, around CB providing better dispersion stability than the polymeric dispersant. AF4-DLS fractograms showed a linear relationship between signal versus concentration. Moreover, the hydrodynamic sizes were analyzed by DLS, both coupled to AF4 and in batch mode, obtaining comparable values. However, the hydrodynamic size showed significant differences in the function of dispersant used for all CB samples assayed, which was related with their different capacities of dispersion. Smaller sizes were obtained and higher amounts of CB were dispersed using biological dispersants, which were improved in a biological medium supplemented with a dipeptide. Good linear calibration graphs were obtained too. Precision studies were also carried out, and the obtained RSD values were lower than 5% for all dispersants.

A stability test with time was carried out, and the results indicated that the biological dispersant allowed dispersions with suitable stability that remained at least for a week, compared with a lack of stability of the polymeric dispersion. A study of CB dispersion stability in several real environmental waters was carried out. The dispersion stability was dependent of the composition of each water matrix, which showed a greater effect in the case of polymeric dispersion. This is an important result because different waters are used in industries in function of their geographic location and this can influence the CB dispersion stability if polymeric dispersion option is employed.

Therefore, it is proposed that the AF4-UV−vis-DLS system may become a valuable tool for rapid characterization, determination, and stability study of CB dispersions in polymeric and biological dispersants. It is interesting to note that a deeper knowledge about CB dispersions is demanded in both research and industrial applications. The stability of aqueous dispersions of CB NPs is still problematic at an industrial level, especially for those applications that require smaller particles, for example, rubber and pigment industries, due to their greater surface area.

MATERIALS AND METHODS

Reagents and Materials. CB samples (N326, N550, and N722) were obtained from Birla Carbon (Cantabria, Spain).

https://doi.org/10.1021/acsomega.1c04527
ACS Omega 2021, 6, 31822−31830

Styrene and acrylic acid used for preparing the polymeric dispersant were provided from Sigma-Aldrich (Missouri, EEUU). Biological culture media used, DMEM/F-12 (with 15 mM HEPES, sodium bicarbonate, stable glutamine, and sodium pyruvate) and DMEM/F-12 modified (supplemented with L-alanyl-L-glutamine dipeptide), were purchased from Merck (Darmstadt, Germany). Also, Tween 80 used for biological dispersions was provided by Sigma-Aldrich (Missouri, EEUU).

The AF4-UV−vis-DLS liquid carrier was prepared with 0.02% NaN_3 (Panreac, Spain). Methanol (VWR, EEUU) was used for cleaning the AF4 system. Water for all the experiments was purified using a Barnstead Nanopure II system.

Instrumentation. AF4 measurements were performed using an AF2000 MT model purchased from Postnova Analytics Inc. (Germany). The channel was 29 cm long with a 10 kDa regenerated cellulose membrane and a 350 μm channel spacer. The flows were provided by two separate pumps, and the cross-flow was obtained by a separate piston pump, which is constantly adjustable. For all AF4 analyses, the liquid carrier was high-purity Milli-Q water containing 0.02% sodium azide. The injection volume was 20 μL, and the dispersions were ultrasonicated for 5 min before each injection. Detection flow was kept at 0.5 mL·min^{-1} or 1.0 mL min^{-1}. Table S1 summarizes the optimal separation conditions.

The AF4 system was coupled online with a UV−vis detector (SPD-20AV, Postnova, Germany), and the DLS detector was coupled with a temperature control (Nano ZS, Malvern, UK). The UV−vis detector was operated at a wavelength of 254 nm. For DLS detection, the AF4 system was directly interfaced to a Zetasizer without channel split, and the detector flow was set to 0.5 mL·min^{-1} for all fractions.

The morphology was studied with a Hitachi S-4800 scanning electron microscope (SEM) at an accelerating voltage of 10.0 keV over metalized CB solid samples with a mixture of gold and palladium for 30 s. TEM samples were prepared by delivering 10 μL of the CB dispersion onto a carbon-coated copper grid (300 mesh) and were dried overnight at room temperature. These samples were analyzed using a JEM 1010 from JEOL Ltd. operated at 100 kV.

An optical microscope (ECLIPSE E200LED MV Series, Nikon Corporation, Tokyo, Japan) was employed under bright-field illumination using 10× and 50× objectives. NIS-Elements 4.20.02 software (Nikon Corporation) was used for acquiring the images.

Finally, CB solid characterization was carried out with a Raman fiber optic probe coupled to a Raman spectrophotometer (EEUU) and a laser source from Ocean Optics. The working wavelength was 532 nm, and the spectra were recorded between 1000 and 3500 cm^{-1}.

Preparation of CB Dispersions. Three different CB samples (N326, N550, and N722) were analyzed. According to the specification of the manufacturer, properties such as SSA and OAN were varied as a function of the CB sample. N326 had an SSA of 78 m^2·g^{-1} and an OAN of 72 mL·(100 g) $^{-1}$; N550 had an SSA of 40 m^2·g^{-1} and an OAN of 121 mL·(100 g)$^{-1}$, and N722 had an SSA of 32 m^2·g^{-1} and an OAN of 65 mL·(100 g)$^{-1}$.

The polymeric dispersant was a mixture of styrene and acrylic acid in a ratio of 3:1 in volume. Then, a solution of 0.025% of this mixture in water was prepared. The CB dispersion was carried out after 5 days of dispersant preparation in order to avoid undesirable responses from the dispersant (see Figure S3). A CB dispersion (300 mg·L^{-1}) was prepared for each CB sample. For this aim, the diluted dispersant and adequate amounts of CB were mixed and agitated for 5 min. After this, the dispersion was sonicated for 2 h. The working dispersion was prepared by adequate dilution of the tested dispersant and sonication for 30 min.

The biological dispersant was an aqueous solution containing Tween 80 (0.02%) and DMEM/F-12 (10%) or DMEM/F-12 supplemented. CB dispersions (300 mg·L^{-1}) of each CB sample were prepared following the same procedure described for polymeric dispersions. Different dilutions of these bulk dispersions (1/2, 1/4, and 1/8) were prepared using the biological dispersant. In this case, dilution with nanopure water was also studied by preparing the same concentration dispersion.

The study on environmental water samples was performed by diluting the CB dispersion in polymeric (dilution factor 1/2) and biological (dilution factor 1/8) dispersions in ultrapure, tap, well, and wastewater samples.

■ ASSOCIATED CONTENT

Supporting Information

The Supporting Information is available free of charge at https://pubs.acs.org/doi/10.1021/acsomega.1c04527.

Precision study; data were obtained for three identical samples subjected to similar treatment with each dispersant; results obtained for CB dispersion in biological dispersant without supplementary compounds; AF4 conditions used for optimal separation; and UV−vis spectra of polymeric dispersants at different times of preparation (PDF)

■ AUTHOR INFORMATION

Corresponding Author

Pilar Campíns-Falcó − *MINTOTA Research Group, Departament de Química Analítica, Facultat de Química, Universitat de Valencia, 46100 Burjassot, Spain;* orcid.org/0000-0002-0980-8298; Email: pilar.campins@uv.es

Authors

Lorenzo Sanjuan-Navarro − *MINTOTA Research Group, Departament de Química Analítica, Facultat de Química, Universitat de Valencia, 46100 Burjassot, Spain;* orcid.org/0000-0001-5594-5130

Yolanda Moliner-Martínez − *MINTOTA Research Group, Departament de Química Analítica, Facultat de Química, Universitat de Valencia, 46100 Burjassot, Spain*

Complete contact information is available at: https://pubs.acs.org/10.1021/acsomega.1c04527

Author Contributions

The manuscript was written through contributions of all authors.

Notes

The authors declare no competing financial interest.

■ ACKNOWLEDGMENTS

The authors acknowledge Birla Carbon (Cantabria, Spain) as the CB supplier. This work was supported by EU FEDER, the Gobierno de España MCIU-AEI (CTQ2017-90082-P), and the Generalitat Valenciana (PROMETEO Program 2020/078

and EU FEDER-Generalitat Valenciana (ID-FEDER/2018/049)). L.S-.N. expresses his gratitude for the FPU grant (MCIU-AEI).

REFERENCES

(1) Arduini, F.; Cinti, S.; Mazzaracchio, V.; Scognamiglio, V.; Amine, A.; Moscone, D. Carbon Black as an Outstanding and Affordable Nanomaterial for Electrochemical (Bio)Sensor Design. *Biosens. Bioelectron.* **2020**, *156*, No. 112033.
(2) Hüffer, T.; Wagner, S.; Reemtsma, T.; Hofmann, T. Sorption of Organic Substances to Tire Wear Materials: Similarities and Differences with Other Types of Microplastic. *TrAC Trends Anal. Chem.* **2019**, *113*, 392−401.
(3) Kausar, A. Contemporary Applications of Carbon Black-Filled Polymer Composites: An Overview of Essential Aspects. *J. Plast. Film Sheeting* **2018**, *34*, 256−299.
(4) Goerlitzer, E. S. A.; Klupp Taylor, R. N.; Vogel, N. Bioinspired Photonic Pigments from Colloidal Self-Assembly. *Adv. Mater.* **2018**, *30*, No. 1706654.
(5) Li, Y.; Huang, X.; Zeng, L.; Li, R.; Tian, H.; Fu, X.; Wang, Y.; Zhong, W.-H. A Review of the Electrical and Mechanical Properties of Carbon Nanofiller-Reinforced Polymer Composites. *J. Mater. Sci.* **2019**, *54*, 1036−1076.
(6) International Carbon Black Association https://www.carbon-black.org/uses-of-carbon-black.
(7) Karsek, L.; Sumita, M. Characterization of Dispersion State of Filler and Polymer-Filler Interactions in Rubber-Carbon Black Composites. *J. Mater. Sci.* **1996**, *31*, 281−289.
(8) Oliveira, T. M. B. F.; Ribeiro, F. W. P.; Sousa, C. P.; Salazar-Banda, G. R.; de Lima-Neto, P.; Correia, A. N.; Morais, S. Current Overview and Perspectives on Carbon-Based (Bio)Sensors for Carbamate Pesticides Electroanalysis. *TrAC Trends Anal. Chem.* **2020**, *124*, No. 115779.
(9) Castrovilli, M. C.; Bolognesi, P.; Chiarinelli, J.; Avaldi, L.; Calandra, P.; Antonacci, A.; Scognamiglio, V. The Convergence of Forefront Technologies in the Design of Laccase-Based Biosensors − An Update. *TrAC Trends Anal. Chem.* **2019**, *119*, 115615.
(10) Bacakova, L.; Pajorova, J.; Tomkova, M.; Matejka, R.; Broz, A.; Stepanovska, J.; Prazak, S.; Skogberg, A.; Siljander, S.; Kallio, P. Applications of Nanocellulose/Nanocarbon Composites: Focus on Biotechnology and Medicine. *Nanomaterials* **2020**, *10*, 196.
(11) Karger-Kocsis, J.; Mahmood, H.; Pegoretti, A. All-Carbon Multi-Scale and Hierarchical Fibers and Related Structural Composites: A Review. *Compos. Sci. Technol.* **2020**, *186*, No. 107932.
(12) Shahgaldi, S.; Hamelin, J. Improved Carbon Nanostructures as a Novel Catalyst Support in the Cathode Side of PEMFC: A Critical Review. *Carbon N. Y.* **2015**, *94*, 705−728.
(13) Li, L.; Hu, L.; Li, J.; Wei, Z. Enhanced Stability of Pt Nanoparticle Electrocatalysts for Fuel Cells. *Nano Res.* **2015**, *8*, 418−440.
(14) Horie, M.; Kato, H.; Endoh, S.; Fujita, K.; Komaba, L. K.; Nishio, K.; Nakamura, A.; Miyauchi, A.; Yamamoto, K.; Kinugasa, S.; Hagihara, Y.; Yoshida, Y.; Iwahashi, H. Cellular Effects of Industrial Metal Nanoparticles and Hydrophilic Carbon Black Dispersion. *J. Toxicol. Sci.* **2014**, *39*, 897−907.
(15) Diabaté, S.; Bergfeldt, B.; Plaumann, D.; Übel, C.; Weiss, C. Anti-Oxidative and Inflammatory Responses Induced by Fly Ash Particles and Carbon Black in Lung Epithelial Cells. *Anal. Bioanal. Chem.* **2011**, *401*, 3197−3212.
(16) Xu, Y.; Liu, J.; Du, C.; Fu, S.; Liu, X. Preparation of Nanoscale Carbon Black Dispersion Using Hyper-Branched Poly(Styrene-Alt-Maleic Anhydride). *Prog. Org. Coatings* **2012**, *75*, 537−542.
(17) Yoon, C.; Choi, J. Synthesising Polymeric Dispersants to Apply to Carbon Black Pigmented Mill Bases for Use in Ink-jet Inks. *Color. Technol.* **2020**, *136*, 60−74.
(18) Kim, W.; Bae, J.; Eum, C. H.; Jung, J.; Lee, S. Study on Dispersibility of Thermally Stable Carbon Black Particles in Ink Using Asymmetric Flow Field-Flow Fractionation (AsFlFFF). *Microchem. J.* **2018**, *142*, 167−174.
(19) Hauptman, N.; Klanjšek Gunde, M.; Kunaver, M.; Bešter-Rogač, M. Influence of Dispersing Additives on the Conductivity of Carbon Black Pigment Dispersion. *J. Coatings Technol. Res.* **2011**, *8*, 553−561.
(20) Yoon, C.; Choi, J. Syntheses of Polymeric Dispersants for Pigmented Ink-Jet Inks. *Color. Technol.* **2008**, *124*, 355−363.
(21) Spinelli, H. J. Polymeric Dispersants in Ink Jet Technology. *Adv. Mater.* **1998**, *10*, 1215−1218.
(22) Fang, K.; Yuan, X. Carbon Black Dispersions for Spun-Dyeing of PAN Fibers. In *"New Century, New Materials and New Life" - Proceedings of 2005 International Conference on Advanced Fibers and Polymer Materials, ICAFPM 2005*; 2005; *1*.
(23) Fowkes, F. M.; Jinnai, H.; Mostafa, M. A.; Anderson, F. W.; Moore, R. J. Mechanism of Electric Charging of Particles in Nonaqueous Liquids. *Col. Surf. Reprograph. Technol.* **1982**, *200*, 307−324.
(24) Liu, K.; Wan, B. An SDS-PAGE Based Method for the Quantification of Carbon Black in Biological Samples. *Analyst* **2020**, *145*, 3370−3375.
(25) Zhang, R.; Wu, Q.; Liu, R. Characterizing the Binding Interaction between Ultrafine Carbon Black (UFCB) and Catalase: Electron Microscopy and Spectroscopic Analysis. *RSC Adv.* **2017**, *7*, 42549−42558.
(26) Tang, J.; Cheng, W.; Gao, J.; Li, Y.; Yao, R.; Rothman, N.; Lan, Q.; Campen, M. J.; Zheng, Y.; Leng, S. Occupational Exposure to Carbon Black Nanoparticles Increases Inflammatory Vascular Disease Risk: An Implication of an Ex Vivo Biosensor Assay. *Part. Fibre Toxicol.* **2020**, *17*, 47.
(27) Lee, D.-K.; Jeon, S.; Jeong, J.; Song, K. S.; Cho, W.-S. Carbon Nanomaterial-Derived Lung Burden Analysis Using UV-Vis Spectrophotometry and Proteinase K Digestion. *Part. Fibre Toxicol.* **2020**, *17*, 43.
(28) Kim, H.; Park, K.; Lee, M.-Y. Biocompatible Dispersion Methods for Carbon Black. *Toxicol. Res.* **2012**, *28*, 209−216.
(29) Zhu, J.; Xiong, Z.; Zheng, J.; Luo, Z.; Zhu, G.; Xiao, C.; Meng, Z.; Li, Y.; Luo, K. Nitrogen-Doped Graphite Encapsulated Fe/Fe3C Nanoparticles and Carbon Black for Enhanced Performance towards Oxygen Reduction. *J. Mater. Sci. Technol.* **2019**, *35*, 2543−2551.
(30) Liu, C. Y.; Cheng, W. T. Surface Modification and Characterization of Carbon Black through Oxidation. *Surf. Interface Anal.* **2019**, *51*, 316−325.
(31) Jiang, Q.; Wang, S.; Xu, S. Preparation and Characterization of Water-Dispersible Carbon Black Grafted with Polyacrylic Acid by High-Energy Electron Beam Irradiation. *J. Mater. Sci.* **2018**, *53*, 6106−6115.
(32) Wang, L.; Zhang, L.; Wang, D.; Li, M.; Du, C.; Fu, S. Surface Modification of Carbon Black by Thiol-Ene Click Reaction for Improving Dispersibility in Aqueous Phase. *J. Dispersion Sci. Technol.* **2019**, *40*, 152−160.
(33) Smiechowski, M. F.; Lvovich, V. F. Characterization of Non-Aqueous Dispersions of Carbon Black Nanoparticles by Electrochemical Impedance Spectroscopy. *J. Electroanal. Chem.* **2005**, *577*, 67−78.
(34) Bott, J.; Franz, R. Investigations into the Potential Abrasive Release of Nanomaterials Due to Material Stress Conditions—Part B: Silver, Titanium Nitride, and Laponite Nanoparticles in Plastic Composites. *Appl. Sci.* **2019**, *9*, 221.
(35) Bott, J.; Franz, R. Investigations into the Potential Abrasive Release of Nanomaterials Due to Material Stress Conditions-Part A: Carbon Black Nano-Particulates in Plastic and Rubber Composites. *Appl. Sci.* **2019**, *9*, 214.
(36) Sanjuan-Navarro, L.; Boughbina-Portolés, A.; Moliner-Martínez, Y.; Campíns-Falcó, P. Aqueous Dilution of Noble NPs Bulk Dispersions: Modeling Instability Due to Dissolution by AF4 and Stablishing Considerations for Plasmonic Assays. *Nanomaterials* **2020**, *10*, 1802.

https://doi.org/10.1021/acsomega.1c04527
ACS Omega 2021, 6, 31822−31830

(37) Jang, M.-H.; Lee, S.; Hwang, Y. S. Characterization of Silver Nanoparticles under Environmentally Relevant Conditions Using Asymmetrical Flow Field-Flow Fractionation (AF4). *PLoS One* **2015**, *10*, No. e0143149.
(38) Bae, J.; Kim, W.; Rah, K.; Jung, E. C.; Lee, S. Application of Flow Field-Flow Fractionation (FlFFF) for Size Characterization of Carbon Black Particles in Ink. *Microchem. J.* **2012**, *104*, 44−48.
(39) Pawlyta, M.; Rouzaud, J.-N.; Duber, S. Raman Microspectroscopy Characterization of Carbon Blacks: Spectral Analysis and Structural Information. *Carbon N. Y.* **2015**, *84*, 479−490.
(40) Mohapatra, S.; Nando, G. B. ANALYSIS OF CARBON BLACK−REINFORCED CARDANOL-MODIFIED NATURAL RUBBER COMPOUNDS. *Rubber Chem. Technol.* **2015**, *88*, 289−309.
(41) Zumdahl, S. S.; Zumdahl, S. A. Chemical Principles, 7th Edition. In *Evolution*; Houghton Mifflin, 2007; 88.
(42) Nel, A. E.; Madler, L.; Velegol, D.; Xia, T.; Hoek, E. M. V.; Somasundaran, P.; Klaessig, F.; Castranova, V.; Thompson, M.; Nel, A. E.; Mädler, L.; Velegol, D.; Xia, T.; Hoek, E. M. V.; Somasundaran, P.; Klaessig, F.; Castranova, V.; Thompson, M. Understanding Biophysicochemical Interactions at the Nano-Bio Interface. *Nat. Mater.* **2009**, *8*, 543−557.
(43) Monopoli, M. P.; Åberg, C.; Salvati, A.; Dawson, K. A. Biomolecular Coronas Provide the Biological Identity of Nanosized Materials. *Nat. Nanotechnol.* **2012**, *7*, 779−786.
(44) Wissler, M. Graphite and Carbon Powders for Electrochemical Applications. *J. Power Sources* **2006**, *156*, 142−150.
(45) *ISO 4656:2012. Rubber Compounding Ingredients - Carbon Black - Determination of Oil Absorption Number (OAN) and Oil Absorption Number of Compressed Sample (COAN).*

https://doi.org/10.1021/acsomega.1c04527
ACS Omega 2021, 6, 31822−31830